ECOLOGICAL MODELLING 199 (2006) 23–38

available at www.sciencedirect.com

ScienceDirect

journal homepage: www.elsevier.com/locate/ecolmodel

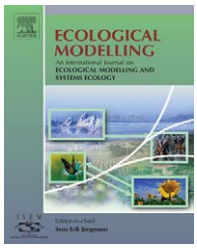

Modelling dwarf mistletoe at three scales: life history, ballistics and contagion

Donald C.E. Robinson[a,*], *Brian W. Geils*[b]

[a] *ESSA Technologies Ltd., Vancouver, BC, Canada*
[b] *USDA Forest Service, Rocky Mountain Research Station, Flagstaff, AZ, USA*

ARTICLE INFO

Article history:
Received 23 February 2006
Received in revised form
6 May 2006
Accepted 16 June 2006
Published on line 8 August 2006

This paper is dedicated to the memory of Frank Hawksworth.

Keywords:
Arceuthobium
Spatial model
Epidemiological model
Forest model
Forest vegetation simulator

ABSTRACT

The epidemiology of dwarf mistletoe (*Arceuthobium*) is simulated for the reproduction, dispersal, and spatial patterns of these plant pathogens on conifer trees. A conceptual model for mistletoe spread and intensification is coded as sets of related subprograms that link to either of two individual-tree growth models (FVS and TASS) used by managers to develop silvicultural and land management plans. This dwarf mistletoe model is based on knowledge of mistletoe biology and forest practices acquired through a series of workshops, programming exercises, and continuing research and development. Key components of mistletoe epidemiology are identified as life history, ballistics, and contagion. An infestation is quantified at the tree-level by a standard measure of mistletoe intensity, the dwarf mistletoe rating (DMR). Life history describes the progression of mistletoe populations from new infections to seed-producing plants and includes biocontrol and mortality of the mistletoe. The model tracks mistletoe populations as changes in DMR rather than individual plants. Life history is represented as changes in pools for various developmental stages; and rates of change are modified by time, light, and other environmental factors (including hyperparasites). Dwarf mistletoes disperse by explosive discharge of small seeds followed by ballistic flight that displaces seeds horizontally to a maximum distance of about 14 m. The model represents dispersal as probabilistic, spatially explicit, ballistic trajectories for each host tree in a simulated stand. The spacing of trees and mistletoe within infested stands exhibits a range of patterns as regular, random, or clumped; the rates of spread to new hosts and intensification within infested hosts are influenced by crown and canopy distributions derived from descriptors of stem clumping and mistletoe contagion. Spatial arrangements of trees in the model are determined from stand-level statistics that characterize groups of trees at the scale of a 14 m radius neighborhood, the maximum distance for ballistic dispersal. The number of trees in a simulated neighborhood is a function of the variance to mean ratio for tree density in the stand. The autocorrelation of trees of more similar DMR is used to simulate aggregation of infected trees into infestation patches. Model behavior for sensitivity to key relationships and fit to observed stands is demonstrated using data for a dense western hemlock stand and two initially similar, open-canopy ponderosa pine stands either treated for mistletoe or left untreated. The model provides a practical tool for assessing the long-term, cumulative effects of disease and management in mistletoe-infested stands.

* *Corresponding author*. Tel.: +1 604 535 1997; fax: +1 604 535 1778.
E-mail address: drobinson@essa.com (D.C.E. Robinson).
0304-3800/$ – see front matter © 2006 Elsevier B.V. All rights reserved.
doi:10.1016/j.ecolmodel.2006.06.007

1. Introduction

Issues of scale are among the first and most important to be addressed by any model. This is true of ecology (Allen and Starr, 1982) and especially true for the epidemiology of the dwarf mistletoes (*Arceuthobium*). These plants, parasites of coniferous trees, have a complex life history spanning a broad range of temporal and spatial scales (Hawksworth and Wiens, 1996) that need to be simultaneously considered before answering even the simple question—how fast does an infestation increase.

We describe here a conceptual and numerical model that represents the epidemiology of dwarf mistletoe (herein simply referred to as mistletoe) at three distinct scales. At the smallest spatial scale the distribution, growth, fruiting and survival of individual mistletoe plants are modeled as life history. Second, the dispersal of mistletoe seeds is represented as ballistics at the scale of the host crown and near neighbors. Finally, the spatial patterns of host and mistletoe distributions are quantified as contagion at the largest scale. The approaches used to simulate events at these three scales are remarkably different from one another. Although the linkages between scales are complementary by necessity and design, the differences show a remarkable divergence in what is necessary to formulate an epidemiological model that effectively bridges scales ranging from a cryptic plant to a forest landscape.

The conceptual model has been implemented as a computer simulation program and linked to two individual-tree growth models, FVS and TASS (see below). Numerically modeling the dispersal of dwarf mistletoes provides two benefits. First, it identifies alternative perspectives and challenges to the understanding of invasive species, disease progression, and spatial patterns of mistletoes and their hosts. Second, the model also provides practical insights on the interplay between stand management – silviculture and disease control – and mistletoe spread and intensification. Because dwarf mistletoe plants require a living conifer host, they are susceptible to control through manipulation of stand characteristics such as composition, spacing, and tree growth (Parmeter, 1978). The model is useful in stands managed for timber production, fire risk reduction, wildlife protection and other situations where successful management requires appropriate silviculture based on an accurate forecast of forest development.

Stand development and disease progression are interactive, complex, and long-term. Almost a century ago, Korstian and Long (1922) characterized dwarf mistletoe as 'an insidious and destructive pest' of ponderosa pine (*Pinus ponderosa*). Since that time, dwarf mistletoes have been recognized as capable of causing significant ecological effects and economic losses. These effects and losses are reviewed by Hawksworth and Shaw (1984) who list the types of damage caused by dwarf mistletoes, identify the important commercial conifer species affected, and provide estimates of the extent and magnitude of losses in western North America. More recently, Watson (2001) presents a summary of the ecological roles and importance of the global mistletoe floras (Loranthaceae and Viscaceae). Hawksworth and Wiens (1996) synthesize fundamental information on the biology and pathology of dwarf mistletoes; this information is recently updated and abbreviated for a more general readership by Geils et al. (2002).

Effective silviculture planning over a multi-decade time scale requires assessments of current stand conditions coupled with forecasts of expected stand structures and health under alternative treatment scenarios (Muir and Geils, 2002). Because of the economic impacts already mentioned, there have been numerous attempts to create quantitative models for evaluating management plans. Several early models of dwarf mistletoe spread and intensification include: Myers et al. (1971), Strand and Roth (1976), Dixon and Hawksworth (1979), Bloomberg et al. (1980), Baker et al. (1982) and Edminster et al. (1990). These models are generally limited in geographic and species scope and in the stand structures and treatments simulated. With the adoption of the Forest Vegetation Simulator (FVS; see Stage, 1973; Dixon, 2002) as the standard, forest stand-projection model in the United States, a need was identified to include dwarf mistletoe effects. Assisted by a series of workshops and modelling exercises (McNamee et al., 1990; Robinson and Sutherland, 1993, 1995; Robinson et al., 1994), empirical relationships were incorporated into FVS to simulate mistletoe intensification and effects on tree survival and growth. Hawksworth et al. (1995) describe the resulting Dwarf Mistletoe Impact Model (DMIM). Chen et al. (1993) provide a sensitivity analysis of that model, and Marsden et al. (1993) demonstrate its application. More recently, Maffei et al. (1999) document a deficiency in the original DMIM for stands of complex structure and propose an enhancement using the empirical logistic approach of Geils and Mathiasen (1990). The current version of the DMIM (David, 2005) is implemented with non-spatial functions to predict change in mistletoe intensity with logistic functions of initial mistletoe intensity, host height growth rate, stand density, and crown class as overstory or understory.

The workshops that defined the scope, objectives and approaches for the non-spatial DMIM extension to FVS also formulated the design for a spatial–statistical model (Robinson and Sutherland, 1995) upon which the epidemiological model described here is based. Although FVS is a non-spatial, distance-independent, individual-tree model, some spatial information is available from sample plots, enabling FVS to simulate stands with patchy structures (Crookston and Stage, 1994). This plot information is combined with a statistical model describing the distribution of host trees by mistletoe intensity within small neighborhoods, and forms the core of the model to simulate mistletoe population dynamics and dispersal. The model has also been linked to a research version of TASS (Tree and Stand Simulator; Mitchell, 1975). In contrast to FVS, TASS is explicitly spatial in both tree locations and in branch growth and geometry; therefore, linkage to TASS excludes the statistical components for approximating stem and mistletoe distributions. Two recent enhancements to the spatial–statistical model include extension for spread between stands (Robinson et al., 2002) and addition of biological control (Robinson et al., 2003).

The population dynamics and epidemiology of dwarf mistletoes are unlike most pathogens in that they are plants, not fungi. Unlike most vascular plants, dwarf mistletoes depend on the photosynthesis of a living host and possess an unusual, hydrostatic seed discharge and ballistic dispersal.

Other models for spread of invasive species, seed dispersal, plant diseases or spatial patterns can provide some general guidance but not to the extent of an integrated, application suitable for silviculture of mistletoe-infested stands. For example, Higgins et al. (2001) describe a process-based, spatially explicit model for invasive plants and identify parameterization and validation as significant challenges. Okubo and Levin (1989) present a framework for comparing seed dispersal curves. Although the trajectory of mistletoe seeds is affected by wind, their dispersal distance is very short compared to seeds modified for extended flight. Willocquet and Savary (2004) demonstrate an epidemiological simulation model at the scales of infection sites, leaves, and plants; their approach is best suited to annual foliage diseases caused by fungi.

We illustrate application of the model to a dense-canopy, old growth, western hemlock (*Tsuga heterophylla*) stand at the Wind River Canopy Crane, Washington, USA (WRCC) and to two, open-canopy, regenerating, ponderosa pine stands near the south rim of the Grand Canyon, Arizona, USA (GC). Information for dwarf mistletoe distribution within tree crowns, and the presence of well-delimited infestation patches at the WRCC allow us to contrast model simulations with alternative assumptions of host and mistletoe distributions. The two GC stands have been either treated by pruning and felling or left as an untreated reference plot, and monitored over the past 50 years. These stands allow us to contrast stand development and disease progression and to compare observed and simulated projections.

2. Natural history

2.1. *Establishment, growth, reproduction and mortality*

The life history of southwestern dwarf mistletoe (*Arceuthobium vaginatum* subsp. *cryptopodum*) is well documented (Hawksworth, 1961) and serves as the archetype for mistletoe life history. Dwarf mistletoes are long-lived plants that may persist for many decades. Because dwarf mistletoes rely upon the host for nutrition, and because reproductive success does not require annual seed production, they can survive without aerial shoots almost invisibly as cryptic infections. Little is known of the physiological mechanisms that regulate shoot production, but it appears that shoot development is suppressed in the low light and nutrition environment of shaded lower crowns (Bickford et al., 2005). Opening the canopy by removing surrounding trees, as is often done to thin or regenerate a stand, commonly results in a proliferation of mistletoe shoots and infections on the residual trees.

The dwarf mistletoe life cycle proceeds through the processes of germination, infection, vegetative growth of the endophytic system and aerial shoots, flowering, fruit maturation, seed dispersal, and inoculation (Hawksworth, 1961; Hawksworth and Wiens, 1996). Although the seeds of southwestern dwarf mistletoe germinate soon after dispersal in late summer, those of most temperate species germinate the following spring when light, moisture, and temperature are suitable. Germination success varies from 7 to 90% and is influenced by physiology, predation, and the abiotic environment. Although little is known about mechanisms of host resistance to infection, a high degree of host specificity and inherited variation in susceptibility suggest that physiological compatibility is required. In a latent phase, before appearance of external symptoms and signs, a mistletoe plant forms the strands and sinkers of the endophytic system which provides the parasite with a nutrient connection to the host. With sufficient growth and a suitable host-environment, the mistletoe produces flowering, aerial shoots. The time from infection to appearance of shoots ranges from 2 to 12 years but is typically about 3–4 years; another 1–2 years are required for flower production. One to several flower crops may be produced over the 2–7-year lifetime of an individual shoot. Dwarf mistletoes are dioecious; most species exhibit a 1:1 sex ratio. Pollen is dispersed by wind or insects; and because mistletoe plants are clustered, pollen is seldom limiting. Although fruit maturation in some tropical species occurs in as few as 4–5 months, most North American species require 12–19 months from flowering to seed dispersal.

Over decades, the pathological effects of infection by dwarf mistletoe (Hawksworth and Wiens, 1996) become evident as the infected branches develop unusual forms (witches' brooms) and are not self-pruned. Although a single, systemic infection can eventually develop into a large broom and constitute most of the live volume within a crown-third, severe pathological effects typically result from infections by numerous mistletoe plants. Although an infection can occur close enough to the trunk to establish a persistent, bole canker, these infections are less effective inoculum sources than branch infections. Unless they break off or are burned off, large infected branches in the lower crown usually remain alive and infected for the life of the host (especially when the host is a pine or Douglas-fir, *Pseudotsuga menziesii*). In contrast, infected branches in the upper crown may thin and die back when the tree becomes severely infested with many infections. Two indigenous species of hyperparasitic fungi (*Colletotrichum gloeosporioides* and *Neonectria neomacrospora*) are able to temporarily suppress or kill western hemlock and lodgepole pine dwarf mistletoes (*Arceuthobium tsugense* and *A. americanum*, respectively). These or other fungi and several herbivorous insects may provide some biological control of dwarf mistletoe (Shamoun et al., 2003).

2.2. *Ballistic seed dispersal*

Seed dispersal begins with the hydrostatic explosive discharge of a single seed from the mature fruit, launching the seed into high-speed ballistic flight. Unlike other mistletoes that are primarily dispersed by birds, dwarf mistletoes rely almost exclusively on this ballistic mechanism. Birds and mammals serve as important but infrequent vectors for the long-distance dissemination of seeds that establish new infestation centers (Nicholls et al., 1991). The viscous seeds are ejected at nearly 24 $m\,s^{-1}$ (Hinds and Hawksworth, 1965; Hawksworth, 1973) and tumble during flight. The trajectory is influenced by height above the ground, fruit orientation at the time of discharge, seed shape and weight, discharge velocity, and gravity (Hawksworth, 1961). Mistletoe seeds have a mass of 2–3 mg, and their flight is altered by wind. With or without wind, seeds reach their final destination within seconds. Although maxi-

mum horizontal displacement can reach 16 m, 10 m is a more typical maximum; and most seeds are displaced horizontally only 2–4 m before interception. Most seeds are deposited lower in the crown; but depending on the discharge angle, some are shot higher.

Because of variation in crown density, foliage, and mistletoe position, seed interception is highly variable. Typically, about 60% of seeds end up on the ground. Of the 40% that are captured in the canopy, 60–80% of these are retained in the crown from which they originate. Of the seeds intercepted in the originating or nearby crown, 90% land on needles (Hawksworth, 1965; Smith, 1985). After ballistic flight, seeds may be moved further by gravity or rarely by birds and mammals (Nicholls et al., 1991). The viscin coat helps seeds adhere to surfaces such as conifer needles, and it later absorbs water, allowing the seed (if properly oriented) to slide to the base of the needle and lodge on the twig. There, the seedling forms a holdfast and a penetration peg by which the parasite enters the host (images by R.F. Scharpf on page 11 of Hawksworth and Wiens, 1996 and also see Brandt et al., 2005). Although fewer than 10% of seeds reach suitable inoculation sites (on a twig at the base of a needle), losses are offset by the large number of seeds produced (Hawksworth, 1965, 1973; Wicker and Shaw, 1967; Smith, 1973).

2.3. *Contagion*

Ballistic dispersal of dwarf mistletoe results in short-range dissemination only, and survival requires a living host. As a consequence, mistletoe plants are clustered within host trees according to the local light and canopy density environment (Shaw and Weiss, 2000; Bickford et al., 2005). Infested patches may range in size from a few trees to many hectares. Such patterns are frequently reported (Dixon and Hawksworth, 1979; Reich et al., 1991), and occasionally quantified by spatial autocorrelation (Robinson et al., 2002; Shaw et al., 2005). Shaw et al. (2005) interpret the pattern of infection patches as the result of founder effects from the initial points of infection. In the absence of screening by non-host species or other barriers, or disruption by other disturbances, patches may eventually coalesce and become indistinguishable over time.

Several studies describe spatial patterns of dwarf mistletoe distribution using a variety of analytical approaches—a multi-response permutation procedure (Reich et al., 1991), spatial autocorrelation with variograms (Maloney and Rizzo, 2002), and Ripley's *K* (Shaw et al., 2005). Although these statistics indicate that distributions may show aggregation, dependency, or contagion, the statistics are descriptive and more useful for interpretation than simulation.

3. Model structure

The concepts of spread and intensification are fundamental for plant disease epidemiology (Seem, 1984). The establishment of mistletoe infection in previously uninfected trees is referred to as *spread*; the establishment of more infection within already-infected trees is *intensification*. Although these two concepts are useful for interpretation of model behavior, distinguishing between them is unnecessary for model construction. Spread and intensification are complementary aspects of the same processes and are influenced by the same factors of inoculum source, tree and crown density, vertical crown structure, and stand species composition.

Dwarf mistletoe plants (a.k.a., *infections*) are usually clustered within groups of trees, referred to as infestation patches. Although infestations can be quantified by the area of patches (e.g., Dixon and Hawksworth, 1979), mistletoe is more commonly described with measures of intensity, severity, and incidence. The standard descriptor of intensity is the dwarf mistletoe rating (DMR; Hawksworth, 1977), a relative index of abundance of mistletoe plants by thirds of a host crown (also see Parker and Mathiasen, 2004). To estimate DMR, the live crown is first visually divided into thirds of equal length. Each crown-third is then rated 0 if not visibly infected, 1 if infected but fewer than half of the branches are infected, or 2 if more than half the branches are infected. Crown-third DMR values are summed to obtain the tree-DMR (integers 0–6). Tree-DMR values are averaged for all susceptible trees in a stand to compute the stand-DMR (rational numbers 0–6). Tree-DMR values averaged for only the infected trees provide a measure of mistletoe severity, DMI (dwarf mistletoe index; Geils and Mathiasen, 1990). The fraction of susceptible trees infected (FINF) describes mistletoe incidence (alternatively, presented as % Infected). By the identity formulation (Eq. (1)), average DMR is also the product of severity and incidence:

$$\mathrm{DMR} = \mathrm{DMI} \times \mathrm{FINF} \quad (1)$$

Although intensity, severity and incidence are useful descriptors, they are not sufficient for projecting future dwarf mistletoe distributions, especially in stands with complex structure. In this model, dwarf mistletoe dispersal is the outcome of spatial relationships involving infected and uninfected trees as sources, targets, or screens. Height and canopy relationships are explicit at the crown-third level, with a 2 m grid-system resolution imposed for some calculations. In the FVS implementation, stem locations are statistical, based on known or assumed spatial relationships between individual trees at the neighbor scale of 14 m radius (maximum dispersal distance). In the TASS model, locations are explicit at the same 2 m resolution. The spatial detail in the model makes it suitable for simulating infection dynamics in multi-species, multi-storied stands and where stand management alters species mix, size distribution, or crown profile. It does not model long-distance dispersal, but is confined to spread and intensification from ballistic flight. The model also does not simulate formation of witches' brooms, nor does it track these as distinct from other infected branches. Users are provided with the means to calibrate many of the model's parameters (Hawksworth et al., 1995).

The spatial dynamics of dispersal operate across a range of scales, from within-tree to neighborhood to stand and beyond. To accommodate this broad range, the model uses three levels of spatial resolution. The model simulates the process and outcome of dispersal separately from the impacts of infection. It was initially designed for – but is not limited to – linkage with FVS to provide a well supported and documented system including user interface and projections of tree growth, tree survival, effects of mistletoe, management and various distur-

bances. Conceptually, the epidemiology model operates with one initialization step, five simulation steps that recur every annual model time-step, and a one linkage step that returns information back to the growth model:

- initialize crown-third distribution from inventory,
- establishment, growth, reproduction and mortality,
- light transmission and opacity,
- ballistic seed dispersal,
- contagion: stem clumping,
- contagion: infestation patches,
- linkage to the growth model.

Crown shapes as height profiles are computed each time-step from species and stand-structure dependent relationships described by Moeur (1985) and used to determine volume for each crown-third. The breakpoints defining crown-thirds move as trees grow and crowns change length. This potentially allows trees to outgrow dwarf mistletoe infections in the upper crown and to create new and uninfected tops. Mistletoe infections do not move with the changing breakpoints but are recalculated to account for changes in the absolute position of each crown-third.

The model makes the simplifying assumptions that dwarf mistletoe infections are distributed evenly within an infested crown-third and that observed crown-third DMR is directly proportional to mistletoe density: mistletoe per unit of crown volume. For internal model use, crown-third DMR (mistletoe m^{-3}) is multiplied by crown-third volume (m^3); thus mistletoe intensity is represented in units of DMR as a rational value, not restricted to 0, 1, or 2 for a crown-third. By definition, a crown-third DMR of 1 represents a minimum abundance of 1 infected branch; and a DMR of 2 represents a minimum abundance of 50% of branches infected. By extension of this concept and for internal model use only, the maximum capacity or full mistletoe occupancy for a crown-third is three DMR-units. New infection (N) added through dispersal is constrained by the amount of mistletoe already in the crown-third so that DMR does not exceed 3 (Eq. (2)). When the crown-third is empty (initially uninfested) there is no constraint on the addition of new infection, but as the crown-third fills the further addition of new infection declines asymptotically to zero.

$$DMR_{t+1} = DMR_t + (3 - DMR_t)(1 - e^{(-1/3N_t)}) \quad (2)$$

After dispersal is projected, crown-third DMR-units (rational values) are converted to tree-DMR (integer values) for reporting purposes. This is accomplished by probability-weighted truncation followed by summing of the crown-third values. If crown-third DMR after dispersal exceeds a value of 2, the rating is truncated to 2.0. Below this ceiling, the crown-third rational value is randomly assigned to the higher or lower integer based on its proximity to the integer. For example, a crown-third with a DMR of 1.31 is rounded down to DMR 1 in 69% of cases, and rounded up to DMR 2 in 31% of cases.

3.1. *Initialize crown-third distribution from inventory*

Standard forest inventories usually provide information for modeling tree growth, including an estimate of DMR observed on sample trees. These, however, usually do not include ratings for each crown-third, so the model assumes a default crown-third ordering for each DMR class (Fig. 1) based on bottom-first filling (Shaw et al., 2005) as the most typical pattern. Model users can modify this initial order for unusual stand structures and histories.

3.2. *Establishment, growth, reproduction and mortality*

At the finest resolution, the model works at the conceptual scale of the life history for a population of dwarf mistletoe plants within the crown-third (Fig. 2). After establishment (inoculation and infection), the mistletoes progress through two transitional stages – latent (pre-symptomatic) and vegeta-

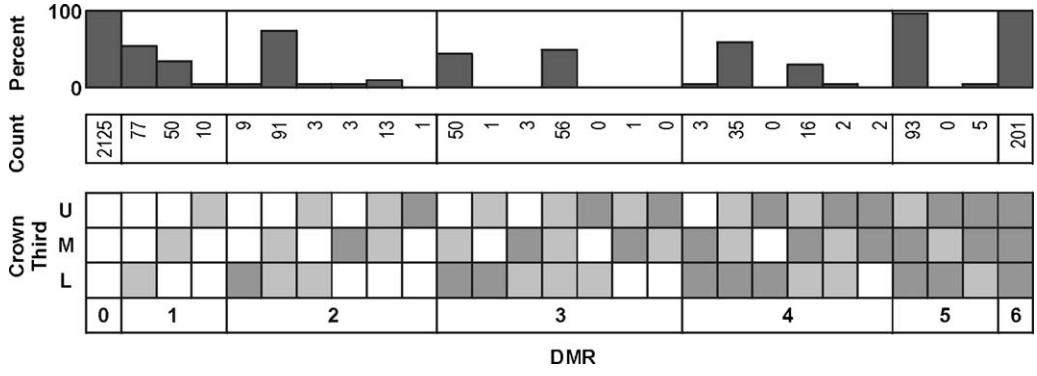

Fig. 1 – Permutations of crown-third mistletoe rating and DMR. The DMR rating of the whole tree may result from various combinations of crown-third rating. The bottom portion shows the permutations that can produce each of the seven DMR classes. Lightly shaded cells indicate a crown-third rating of 1; heavily shaded cells have a rating of 2. The middle section of the figure is based on an inventory of the WRCC stand and shows the number of western hemlock trees observed with each possible permutation; the upper section shows the percentage of the DMR class in each permutation. Inspection of the most frequent crown-third permutation in each DMR class suggests that a "bottom-up" model be used to assign a dwarf mistletoe rating to each crown-third when given only an inventory of tree-DMR. Crown-thirds are: L: lower crown-third; M: middle crown-third; U: upper crown-third.

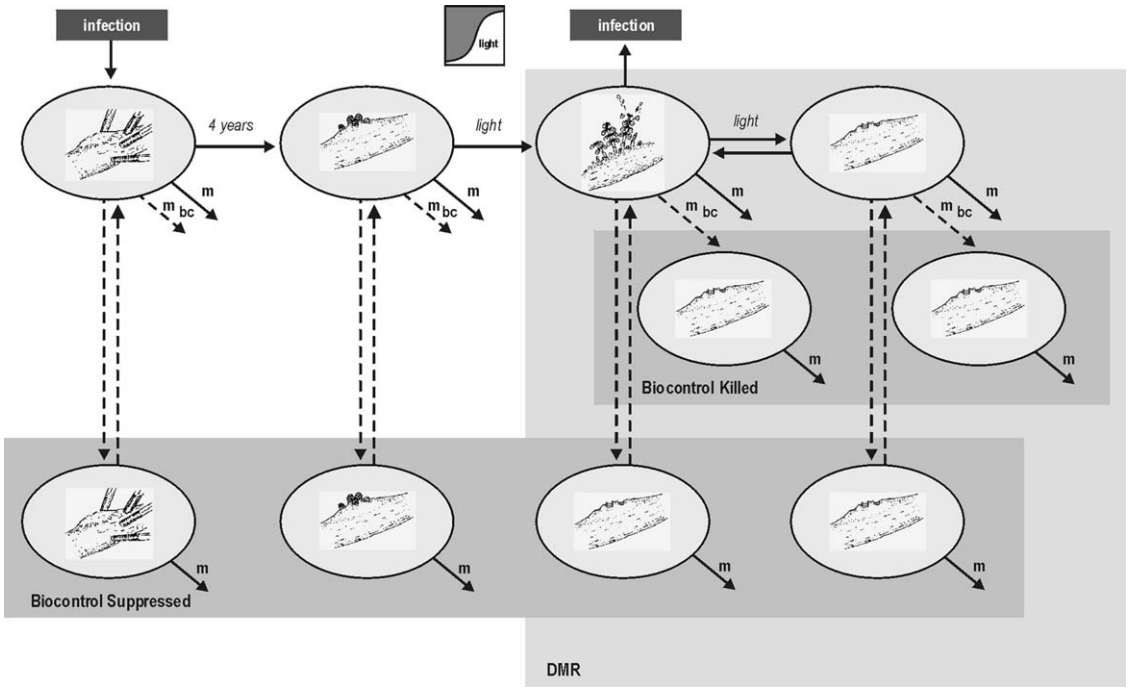

Fig. 2 – Life-history model for dwarf mistletoe. The life-history of dwarf mistletoe (*Arceuthobium*) is divided into four stages, shown left-to-right: latent (pre-symptomatic), vegetative (symptomatic but pre-flowering), reproductive (flowering and fruiting), and suppressed (having been vegetative or reproductive but without live aerial shoots). Biotic agents can temporarily suppress shoots or kill plants at any a stage (bottom row, m_{bc}). Host and environmental conditions can cause natural mortality (m) at all stages. Live, infected branches used to determine the dwarf mistletoe rating (DMR) are identified as those with signs of mistletoe presence (live shoots) or signs (dead shoots or basal cups) on branches with symptomatic swellings, resin, or brooming. Mistletoe in the reproductive and suppressed stages (light gray box) are typically observed and used for rating.

tive (cryptic aerial shoots) – to a reproductive stage (flowering and fruiting) which contributes to production of new infections. Depending on the light environment, a portion of the reproductive population may be suppressed and discontinue reproduction; upon renewal of favorable light conditions, a portion of the suppressed population may return to the pool of reproducing mistletoes. Suppressed infections would be seen as swollen and broomed branches with remains of old mistletoe shoots, so both reproductive and suppressed pools are used to compute the tree-DMR returned to the growth model. To account for mistletoe mortality, temporary reproductive suppression by a biological control agent, and mortality by a biological control agent, several additional pools are recognized into which portions of the mistletoe population transition (see Fig. 2). The amount of infection in these pools and transition between pools are controlled by an initialization process, by seed dispersal into the latent pool, and by various rates set through default values and functions dependent on incident light. By default, 25% of latent infections progress to the vegetative stage each year (representing a typical 4-year latency); this residence can be increased or deceased by the user for populations having an average shorter or longer latent period. In addition to changes in DMR resulting from crown dynamics, each pool is also subject to a default mortality rate of 0.08 year^{-1}. This rate is a workshop consensus value that can be adjusted to calibrate the model to a specific, dwarf mistletoe population if its typical mortality rate were known.

Light triggers two of the transitions between life history stages, and is modeled at the stand level as a height-dependent extinction curve. As described in a subsequent section, this curve is created using a simulated stem map and stand-average transmission of light (the complement of stand-average opacity, see below) computed for each 2-m layer-slice of the stand. The vegetative-to-reproductive transition is modeled using the fraction of incident light reaching each 2-m layer in the crown-third. By default, 100% of vegetative infections will become reproductive each year if 100% of the total available light is present; 50% will become mature if 50% of the available light is present, and so on. Conversely, a reproductive-to-suppressed transition can take place if light levels decline. By default 100% of reproductive infections become suppressed at 0% light, 50% become latent at 50% light, and so on. Model users are able to change both the forward and backward transition functions, and thus change the dynamics of the light response.

A set of calculations based on stand inventory data is made during model initialization to establish initial proportions in each life history pool. The initial light environment is evaluated, and the model executed with its initial crown-third ratings until the proportional infection in each life history pool reaches equilibrium. Then rescaling is performed so that the initial crown-third rating matches the sum of the initial reproductive and suppressed categories. The infection subpools within each crown-third are maintained from time-step

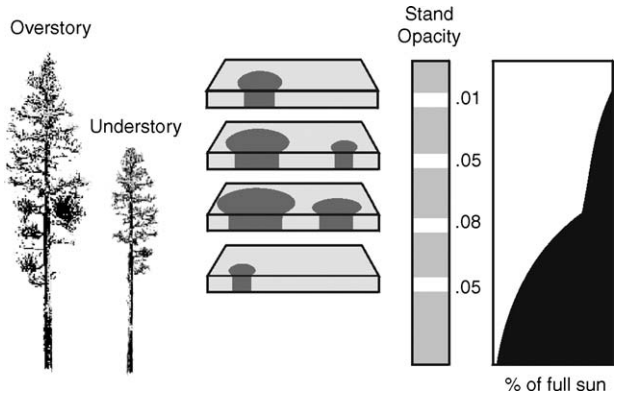

Fig. 3 – Stand-average opacity and light transmission. A stand canopy consists of crowns of different length, shape and density from trees of different species and heights. This complex canopy–gap structure is spatially represented in an epidemiological dwarf mistletoe model as a series of 2-m vertical layers extended upward to 50 m and over a 1-ha area. Using a simulated placement of stand trees with species-dependent crown opacity (relative ability to intercept light and mistletoe seeds), stand-average opacity is computed at 2-m intervals for the generalized stand canopy and used to describe a specific light-extinction curve for the stand.

to time-step. Pools are adjusted to conserve the amount of infection with changing crown volume and shifting crown-third breakpoints that result from the growth of the host tree and change in crown length.

3.3. *Light transmission and opacity*

Stands are composed of trees of different species, heights, crown shapes, crown lengths, foliage density, and spacing. To account for this diversity, opacity is computed by Monte Carlo simulation at each time-step with a 1-ha stand of randomly located trees. Simulation uses species, height, crown length and the geometry relationships described by Moeur (1985) to construct a set of 2-m canopy slices for each tree (Fig. 3). At each 2-m height increment, crown opacity for a tree is computed from the density of stems, branches, and foliage; stand-average opacity is computed from the crown opacities adjusting for tree spacing. The stand-average opacity is used to reduce the amount of light that can be transmitted from the top of the stand to the ground. Because light extinction is cumulative, a decay curve results. Crown opacity and stand-average opacity of this generalized stand canopy are used with ballistic trajectories to model seed interception.

3.4. *Ballistic seed dispersal*

Infested crown-thirds introduce new infection to themselves and their neighbors. Because of physical dynamics of seed flight, infections that leave the host crown are more likely (but not exclusively) to be transmitted outward and downward from an infection source to the crown of a neighboring target tree. Tree height and crown information are used to simulate the height of trees and their neighbors, so that an infection higher in a tree spreads to a neighbor with a lower crown more frequently than an infection low in a crown spreads upward to a taller tree.

The model uses encoded and simplified ballistic trajectories to represent the key spatial aspects of an infected source tree's potential for dispersal within its own crown and to neighboring target trees. Each host tree acts as both a source and target, since neighbors can infect one another. The encoding of simplified trajectories begins with a more detailed trajectory simulation (Eq. (3)) using an initial velocity, v_0, of 24 m s^{-1} and terminal velocity of 7.5 m s^{-1} (Hawksworth, 1959; Hinds and Hawksworth, 1965). The angle of discharge is uniformly distributed from straight up to straight down, and aerodynamic friction is represented as a quadratic function of velocity over the range of speeds experienced during seed flight. Friction is parameterized so that at 7.5 m s^{-1} (terminal velocity) a decelerating drag force of 9.8 m s^{-2} is experienced. Seeds of all dwarf mistletoe species represented by the model are assumed to obey the same trajectory constraints. These relationships were coded in a separate model to simulate the paths generated by 1000 trajectories. These simulations showed that regardless of discharge angle, virtually all horizontal motion is damped by friction after a drop of 20 m from the point of discharge. This means that it is only necessary to simulate trajectories until they drop 20 m; beyond that, seeds are falling straight down. The detailed simulations ignore the potential influence of wind on horizontal displacement and predict a maximum 14 m horizontal flight distance and a maximum 6 m vertical rise. Both these predictions are consistent with field observations (e.g., Hawksworth, 1961).

From the initial conditions described above, each trajectory is computed by calculating seed velocity using a 1 ms time-step:

$$\vec{V}_{t+1} = \vec{V}_t + \vec{F}_t + \vec{G} \quad (3)$$

where F and G are friction and gravity vectors, respectively. Beginning with explosive release from an initial height of 19 m, each of the 1000 simulations produces a trajectory of horizontal (x) and vertical (z) positions describing seed position over time. When all the simulated trajectories are graphed together and crown interception is temporarily ignored, they generate the pattern shown in the left panel of Fig. 4. This figure shows that in the absence of interception, the distribution of seeds landing on the ground is skewed in favor of distances of about 12 m from the source. Moreover, it also shows that outside the immediate vicinity of its point of origination, the highest density of seed rain is experienced near the outer edge of the trajectory envelope.

To make the trajectory simulations faster, the precision of each trajectory location is reduced to a resolution of 2 m. This is done by superimposing a grid over the plane of the trajectories, as shown in the middle and right panels of Fig. 4. The grid extends up along the z-axis to a maximum of 26 m and laterally along the x-axis for 14 m. Each trajectory is then simplified to a sequence of grid cells through which the trajectory passes. Many of the trajectories are so close together that they follow the same sequence of grid cells (center panel). As a consequence, some trajectories are assigned a greater weight to

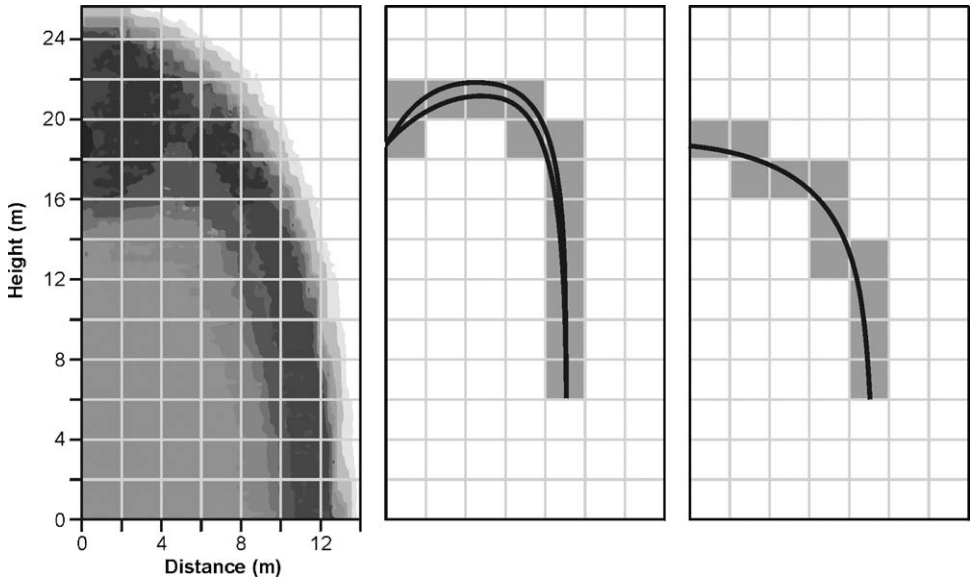

Fig. 4 – Ballistic simulation using 2-m grid. Left panel: 1000 simulated trajectories emanate from a point 19 m above the ground in this example. Darker shading in the left panel indicates higher seed density. Ignoring crown interception effects, dispersal can move seeds upward by as much as 6 m and outward as far as 14 m. Below the source, many trajectories converge 12 m outward from the source, as indicated by the darker shading. Center and right panels: trajectory information is encoded as the unique sequences of grid-squares arriving at each cell. This example shows two different paths both ending in grid cell [5,4] (in this example, 10 m horizontal distance from the source and 8 m above the ground) The trajectories summarized in the center panel have a weight of 2 and those in the right panel have a weight of 1.

signify that they represent multiple paths. A second consequence of the trajectory simulation is that different sets of trajectories can arrive at the same grid-cell endpoint, as shown in the middle and right panels of Fig. 4.

The use of a pre-computed trajectory grid allows us to superimpose the grid at any height within a source tree, shifting the reference frame to account for the actual height of the source infection and scaling its strength by the amount of infection within each 2-m slice of each infected crown-third. To further simplify the model and make it computationally practical, we investigated ways to further reduce the number of trajectories. We began by first removing the 20% lowest weight trajectories arriving in every grid cell, retaining and re-weighting the remaining trajectories. We explored this further and found that we were able to maintain model behavior using only 20% of the original trajectories, or a minimum of 1 trajectory arriving per grid square. The trajectory reduction method preserves the overall amount of infection transmitted from a source tree but reduces the amount of variability in the outcome of the trajectories.

From the reference point of each target grid cell (e.g., cell [5,4] in the center and right panels of Fig. 4), the total number of incoming trajectories is the sum of all the trajectories arriving at the cell. Once crown interception is taken into account, this method correctly calculates the possible effects of trajectories (dispersing seeds) that travel upward and then downward as well as those that travel a more direct path and experience different potential interception encounters. In effect, it performs the integration (albeit at a 2 m resolution) of all possible seed paths between any source cell and target cell. This approach was suggested by Feynman's description (1985, Chapter 2) of weird photon behavior, which provoked the all-possible-paths ideas used here to simulate dispersal trajectories.

Ballistic paths are linked to crown-third infections by assuming that dwarf mistletoe is distributed evenly through the crown-third. Using this simplifying assumption each crown-third is subdivided horizontally (like a layer cake) at 2-m grid boundaries, making allowance for the fact that crown-third boundaries and grid boundaries do not usually coincide. After this division is made, the midpoint of each 2-m slice within each crown-third is used as the point from which all dispersing infections are projected. This step combines crown volume, height and trajectory dynamics. However, it also makes the simplifying assumption that all infections are projected from the stem of the tree. In fact, infections can reside almost anywhere within the crown and seeds can be projected in any direction. A Monte Carlo examination of the effects of this point source assumption indicates that it contributes a small amount of bias; removing the variation that results from having a variety of seed-flight origins underestimates average dispersal by 5%.

The description of dispersal trajectories has so far ignored the fact that tree crowns intercept seeds. Depending on the discharge angle and canopy density within a source tree, some infection may be retained either within the source crown-third or in adjacent crown-thirds. The amount of self-infection is a function of crown opacity, defined as the likelihood of interception during passage through 1 m of crown. The default crown opacity of ponderosa pine is 0.1 and 0.2 m^{-1} for western hemlock (see Hawksworth et al., 1995 for other species). Upon escaping a source crown, seeds may be blocked by screening trees (as a function of the stand-average opacity

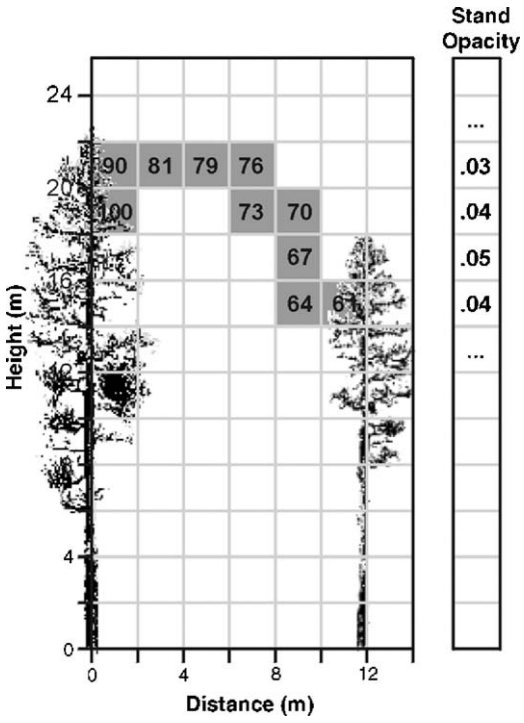

Fig. 5 – Dispersal example. Dispersal and interception of dwarf mistletoe seeds from a source tree (left) to target host tree (right) is modeled as a series of trajectories passing through a source crown, then through generalized stand canopy and into a target crown. The epidemiological mistletoe model simulates the spacing between source and target trees and represents the likelihood of seed interception by source and target trees as a function of their crown opacity. Seeds are also intercepted or screened from reaching the target tree by trees of the generalized stand canopy which combine to determine a stand-average opacity which varies with height (see Fig. 3). In this example, one possible trajectory is traced to illustrate the transfer of mistletoe (as DMR) from a target tree as it passes through multiple 2-m grid cells. Within a source tree with crown opacity of 0.1 per cell, the weighted DMR transfer is reduced from 100 to 81 as it passes through two crown cells (intensifying the infection in the source tree crown). Within the generalized stand canopy, the weighted DMR transfer is reduced for each cell transited by an amount dependent of the average-stand opacity at the cell height. After passage through two source canopy cells and eight stand canopy cells, mistletoe following this trajectory would be reduced to 61% (61/100) of what was produced in the source cell.

of the generalized stand canopy), intercepted by a target tree (as a function of its crown opacity) or fall to the ground.

Dispersal trajectories provide the means of computing the transmission of dwarf mistletoe (as DMR) from a source to a target tree. In Fig. 5 an example trajectory is given an initial weight of 100 with crown opacity set to 0.1 per grid cell. As the trajectory moves upward and outward from the source tree, it initially passes upward through the source crown, traversing two grid cells. When the trajectory emerges from these cells it has a weight of $100 \times (1 - 0.1) \times (1 - 0.1) = 81$. The trajectory then leaves the source crown and enters the generalized stand canopy composed of canopy gaps and crowns of other trees. Its weight is further reduced in each grid square it travels through, simulating the effects of trees that might intercept or screen seeds between a specific target and source. Host and non-host screening trees are not explicitly present between source and target, but are represented through their average effect (stand-average opacity of the generalized stand canopy), an approach that allows the model to avoid simulating the location and role of every tree in the neighborhood while capturing the important observation that spread is reduced in mixed-species stands because of non-host interception of seeds. To continue the example shown in Fig. 5, the stand-average opacity of grid squares along the path between the source and target reduces the trajectory weight from 81 to 61. Entering the target tree crown with a weight of 61, it is then intercepted in proportion to the opacity of the target host. Although the actual path taken through the target crown may vary between a grazing encounter and the full diameter of the target at the height of the 2-m layer-slice, we assume that on average it will pass through a thickness of canopy equal to the radius. Given a crown radius of 1 grid cell at the intersection of the target tree with the trajectory field, the weight of the intercepted trajectory is $61 \times 0.1 = 6.1$. In this way the dispersal trajectory calculations are consistently applied to allow both spread and intensification, and account for the roles of source, target and screening trees.

3.5. *Contagion: stem clumping*

At the scale of the neighborhood, seeds disperse to target trees from infected source trees. In the model, the neighborhood of each target tree is simulated through a relationship that allows stem spacing to be regular, random or clumped. Additionally, the model simulates the patchy distribution of mistletoe as the similarity of DMR among neighbors. Stem spacing is modeled independently of mistletoe distribution, and both are under user control.

The model simulates stem spacing as shown in Fig. 6 by placing a target tree at the center of a bull's-eye of concentric 2-m rings. This representation is consistent with the 2-m grid used to compute opacity and flight trajectories. When the grid system, which is defined in an x–z plane, is rotated around the target, it creates concentric rings in the x–y plane and concentric cylinders in x–y–z. Seven of these concentric rings are simulated around each target. The choice of seven rings results from the observation that in the absence of wind, lateral ballistic flight is rarely more than 14 m. Source trees are selected and simulated as if they were located at the outer edge of each of the concentric rings. Placing targets at the center of the bull's-eye and source trees at discrete distances allows the grid of dispersal trajectories (see Fig. 5) from each source tree to overlap the canopy of the target. The model uses the binomial family (Binomial, Poisson and Negative Binomial) to compute probability distributions of the number of neighbors in each sample ring based on the variance-to-mean ratio for host tree density at the 14 m-radius neighborhood scale. Where appropriately scaled inventory plots or other information are not available, a default random pattern (Poisson) is used.

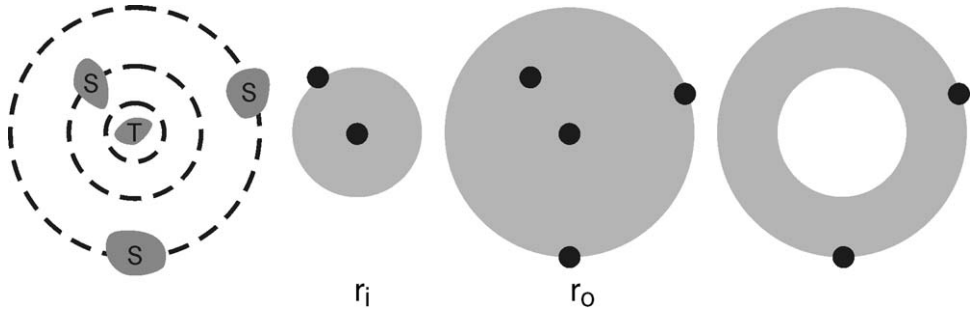

Fig. 6 – Simulated stem clumping. Stem clumping is simulated by placing the target tree (T) at the center of a bull's-eye of concentric rings, each 2 m wide. Depending on the level of dispersion (variance/mean) in the stand, different statistical distributions describe the abundance of neighboring source tree stems (S) in each sample ring. The probability distribution for each sample ring is determined by overlaying the distribution for the inner circle, r_i, with the outer circle, r_o. The differences between them can be used to compute the distribution function for the non-intersecting part, allowing for the fact that samples are not independent. This example shows one way in which a ring sample of 2 could be generated. No specific position within the ring is simulated.

Each concentric ring is defined by its inner and outer radius, r_i and r_o. The expected number of stems within each ring is drawn from the probability distribution of the host species in the following way. The distribution for the disc with radius r_i (the r_i disc) is derived first, giving the probability of sampling $x = 0,1,2,3,\ldots$ trees in the inner disk. The same method is followed for the larger r_o disc, as shown in Fig. 6. The expected distribution of trees in the ring is then defined by the distribution of trees found in disc r_o that are not already in disc r_i. The distribution is calculated by counting all the combinations of tree numbers on the two discs that would give rise to an observation of a particular number of trees in the ring (Eq. (4)). Although the summation continues infinitely, the upper tail of the distribution drops off rapidly and in practice the summation usually includes fewer than 20 terms:

$$P(x = n|r_i, r_o) = \frac{\sum_{j=n}^{\infty} P(x = j|r_o)P(x = j - n|r_i)}{\sum_{k=0}^{\infty}\sum_{j=k}^{\infty} P(x = j|r_o)P(x = j - k|r_i)} \quad (4)$$

Scaling of the ring probability distribution is necessary because the two disc samples are not independent. Since the r_i disc lies completely inside the r_o disc, some tree number combinations are not allowed. For example, if a sample of size 3 were observed in r_i, then a sample of 2 or fewer could never be observed in r_o: the smallest sample that could be found in r_o would also be 3, giving a ring sample size of 0. The double summation in the denominator performs this scaling, so that the sum of probabilities over all sample sizes is 1.

Following this approach, every tree is simulated as a target at the center of a neighborhood with a variable number of other host trees. The number of trees in the neighborhood depends only on the variance to mean ratio of host density at the 14-m neighborhood scale. Once the number of trees in each ring is determined, the choice of neighboring trees depends on the DMR of the target and the spatial autocorrelation of mistletoe distribution. Non-host trees in the neighborhood are not modeled explicitly, but their presence is accounted for through the stand-average opacity effects already described.

3.6. *Contagion: infestation patches*

Within a patch, it is more likely that trees of similar DMR are near one another than trees of dissimilar DMR. We express this relationship using a simple exponential rescaling (Eq. (5)) controlled by the absolute magnitude of DMR difference between a target, DMR_t, and each class of potential source trees, DMR_s. This relationship, applied to the stand-average density of each DMR source class (ρ_s) in the 14-m radius neighborhood of the target, yields the estimate $\rho_{s,t}$ for the density of each class of source trees in the neighborhood of the target. The numerator and denominator terms in Eq. (5) further adjust the density of each DMR class to preserve the stand-average density of each class across the entire range of DMR targets. The exponential coefficient α controls the degree of mistletoe contagion by shifting neighbor density according to the similarity of DMR. For α less than 0, trees of similar DMR are more likely to be neighbors (forming distinct patches); for α greater than 0, trees of dissimilar DMR are more likely to be neighbors than if there were no patch structure (when $\alpha = 0$):

$$\rho_{s,t} = \rho_s \, e^{\alpha|DMR_t - DMR_s|} \frac{\sum_{j=0}^{6} \rho_j}{\sum_{j=0}^{6} \rho_j \, e^{\alpha|DMR_t - DMR_j|}} \quad (5)$$

By design, this relationship does not change the aggregate DMR statistics of the stand (tree density by DMR class). To preserve the stand-level statistics, a reduced chance of finding a source tree that has a DMR that is very different from the target implies an increase in the density of similar-DMR sources in other neighborhoods. Eq. (5) preserves this symmetric property of target–source differences in DMR; trees not in one neighborhood are located in another neighborhood (Table 1).

Analyses of stem-mapped data from the WRCC and GC plots have been used to set a default value $\alpha = -0.5$ for stands where dispersal, reproduction, and mortality have produced a typical, patchy pattern of mistletoe distribution. Model users may set an alternative value for α based on specific inventory data or other knowledge of stand history and mistletoe distribution. A value for α could be estimated by nonlinear regression if a stem map were available or if the stand had

Table 1 – Effect of contagion on the local neighborhood

Source DMR	ρ_s	Target DMR						
		0	1	2	3	4	5	6
0	177	220	193	164	135	107	76	53
1	12	8	21	18	15	12	8	6
2	10	4	11	26	22	17	12	8
3	9	2	6	14	33	26	19	13
4	5	1	2	4	10	22	16	11
5	8	1	2	5	11	24	48	33
6	17	1	2	5	13	29	57	113
Sum	237	237	237	237	237	237	237	237

Density (trees ha^{-1}) of host western hemlock at the Wind River Canopy Crane stand. Stand-average density (ρ_s) of each DMR class for the whole stand is shown at the left. Modeled local neighborhood density ($\rho_{s,t}$) is shown by DMR source-tree class within 14 m radius neighborhoods around target trees of a given DMR, using the observed stand spatial autocorrelation parameter $\alpha = -0.52$ (see text, Eq. (5)).

been inventoried with multiple sample plots (a good design includes about 50 plots of 14 m radius). If treatment or tree regeneration (natural or planted) resulted in mistletoe being evenly spread throughout the stand (no patches), an α-value near 0 could be selected. Alternatively, if there were recognizable patches of infected trees in which groups of more severely infected trees graded into a matrix of less severely infected trees, a more negative α-value from −1.0 to −2.0 could be selected.

3.7. *Linkage to the growth model*

The final step in the simulation is to return to the growth model an updated DMR for each simulated tree record. This DMR is used to modify tree growth and survival (for FVS, see Hawksworth et al., 1995) and is available for suggesting management actions and for simulating activities such as sanitation thinning (Dixon, 2002). All crown-third life history pools (Fig. 2) are maintained across model time-steps and are adjusted for changes in crown position, in preparation for the next time-step. Besides proximity to potential source trees, change in crown-third DMR depends on the rates of success for interception and germination and the weighting of trajectory scaling. Although defaults are provided, these processes are available for tuning as simple multipliers.

4. Model behavior

4.1. *Wind River Canopy Crane sensitivity simulations*

We made a systematic exploration of model behavior through a set of parameter-sensitivity runs using the WRCC stand, linking the model to the West Cascades FVS variant. This 12 ha stand was inventoried in 1995 and is dominated by western hemlock (237 stems ha^{-1}) with lesser amounts (51 stems ha^{-1}) of grand fir (*Abies grandis*) and silver fir (*A. amabilis*). The oldest trees are about 450 years, and stem maps show several patches of western hemlock dwarf mistletoe (see Fig. 10A in Shaw et al., 2005). Initial stand quadratic mean diameter (QMD) is 39 cm with a basal area of 43 m^2 ha^{-1} and top height of 36 m. We computed whole-stand estimates of mistletoe contagion ($\alpha = -0.52$) and stem clumping ($\sigma^2/\mu = 2.2$) using sample quadrats corresponding to a 14 m radius plot. We also used Parker's (1997) estimates of canopy light penetration to parameterize crown opacity at 0.18 m^{-1}, such that light penetration near the ground is about 11% of full-sky illumination.

We systematically varied four parameters in a 50-year simulation: initial crown-third loading, crown opacity, mistletoe contagion, and stem clumping (Table 2 and Fig. 7). The results shown in Fig. 7 use DMR, DMI and % Infected as measures of mistletoe intensity, severity, and incidence. In each scenario, three parameters were held constant at the best-fit value and the fourth was varied to demonstrate model sensitivity. The simulations did not incorporate future regeneration or disturbance mortality (root disease or wind throw) other than the higher mortality experienced by heavily infected host trees.

Three loading scenarios are shown in the first column of Fig. 7. The infection measures are all similar regardless of load-

Table 2 – Parameter values for model sensitivity analyses

	Scenario			
	Loading	Opacity	Contagion	Clumping
Loading	D: top H: bottom L: middle	Bottom	Bottom	Bottom
Opacity	0.18	D: 0.36 H: 0.18 L: 0.05	0.18	0.18
Contagion	–0.52	–0.52	D: −2.0 H: −0.52 L: 0.0	−0.52
Clumping	2.2	2.2	2.2	D: 10.0 H: 2.2 L: 0.01

Model sensitivity to four parameters was demonstrated using the WRCC stand and four scenarios. In each scenario three parameters were held constant and the fourth was varied above and below the best-fit value. Terms and units are defined in the text, and corresponding plots are shown in Fig. 7. D, H, L labels refer to the dotted (more extreme), heavy (best-fit) and light (less extreme) lines shown in Fig. 7.

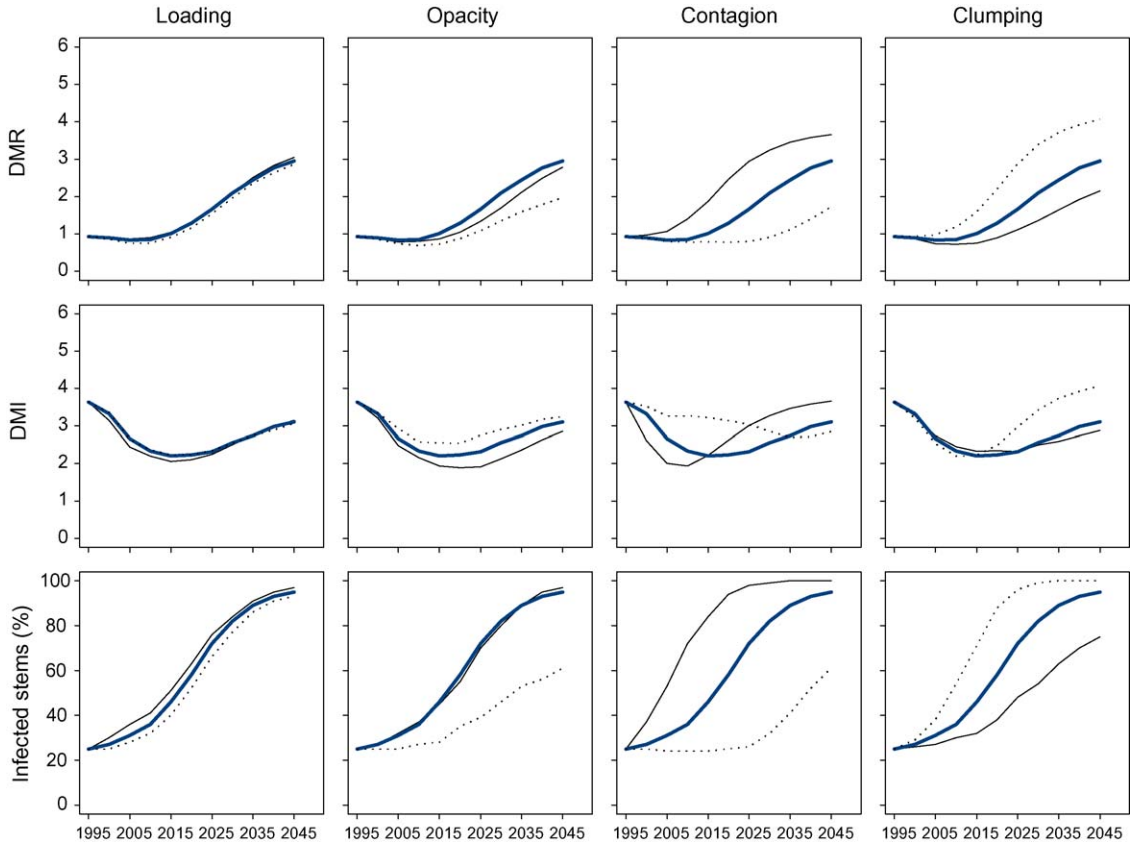

Fig. 7 – Model sensitivity and behaviour in the WRCC stand. Model sensitivity to four variables (loading: initial crown-third loading sequence for inventory DMR; opacity: crown opacity; contagion: spatial autocorrelation of DMR classes; clumping: stem clumping of the host) is shown in four columns for a set of simulations from the WRCC stand. Each column shows a set of three simulations in which the respective column-variable was changed, holding the remaining column-variables constant at their best-fit level. Three lines within each plot show results for the best-fit value (heavy line), compared to results using values that are less (light) and more (dotted) extreme, with the exception of the initial crown-loading scenarios, which are categorical. Note that the best-fit lines are identical within rows.

ing, thereby indicating that for this stand the model is not strongly sensitive to initial mistletoe distribution by crown-third. When crown opacity is varied (second column), a number of model behaviors and outcomes are evident. First, raising opacity reduces spread, because more seed is retained in the crowns of infected trees, making less available for new infections. Moreover, light is reduced, placing more of the population in a non-reproductive state. Both outcomes contribute to a noticeable reduction in spread (fewer trees infected) and slightly increased intensification (infection conserved within previously infected trees; few low-severity trees added) with a net, modest effect on mistletoe intensity (DMR). These effects are not linear however, as shown by the similarity of the medium- and low-opacity simulations.

When mistletoe contagion (third column of Fig. 7) is lowered, the model distributes infected host trees more uniformly and widely throughout the stand. This increases the potential for spread, as reflected by the different trajectories for mistletoe incidence (% Infected). With greater spread relative to intensification, mistletoe severity (DMI) shows a temporary decline, reflecting spread of mistletoe to previously uninfected host trees. As most trees in the stand become infected, the distinction between severity and intensity (DMR) diminishes. When mistletoe contagion is increased, intensification initially dominates over spread until intensification becomes limited by maximum tree-DMR and the most severely infected trees die. Stem clumping (fourth column of Fig. 7) also affects mistletoe incidence and severity. Compared to the observed level of stem clumping, an increase results in less distance between potential new hosts and an increased rate of spread as shown by an initial steep increase for incidence. Once most trees become infected, intensification dominates over further spread, as seen in the delayed rise of severity.

4.2. *Grand Canyon sanitation simulations*

We also explored how well the model is able to simulate tree and mistletoe dynamics in two stands repeatedly inventoried for five decades, linking the model to the Central Rockies variant of FVS. Control of dwarf mistletoe was conducted at Grand Canyon National Park to improve survival of large, old-growth ponderosa pine trees and to reduce mistletoe impacts (Lightle and Hawksworth, 1973). The infested portion of the ponderosa pine forest on the south rim was treated in a series of entries

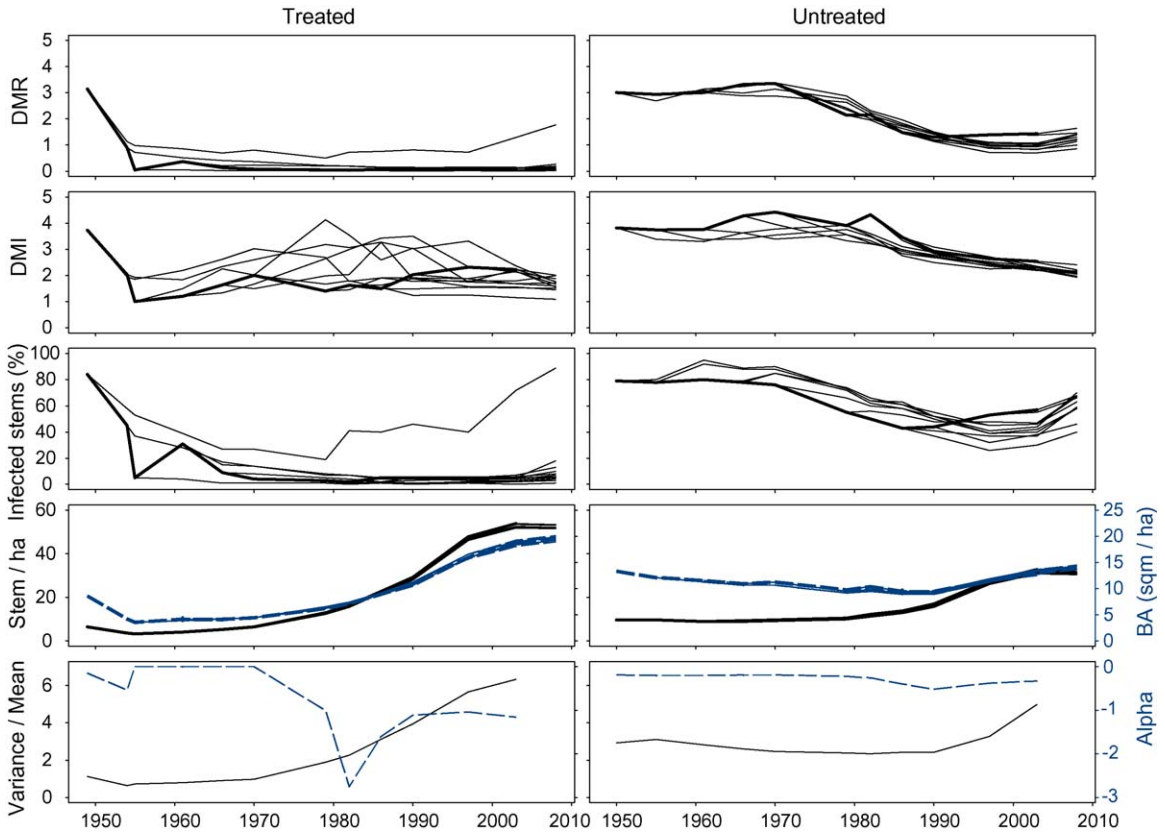

Fig. 8 – Model behaviour in the GC stands. Model predictions are compared against observed inventory in two stands from the Grand Canyon. The stand shown in the left column was treated by pruning or killing infected trees; the stand at the right was untreated. Fine lines in the upper four rows show simulation results starting from each of 12 treated and 11 untreated stand inventories made between 1949 and 2003. Heavy lines connect the inventory data. In the bottom two rows, solid lines correspond to the left scale and dashed lines correspond to the right scale. The upper three rows demonstrate the extent of the model's fidelity to actual stand conditions over a period of five decades. The fourth row shows the close correspondence between predicted and observed change in tree attributes (stem density and basal area) modeled by the FVS growth model. The bottom row shows the input values for levels of stem clumping (left axis) and mistletoe contagion (right axis) used in the simulations.

from 1949 to 1966 by pruning lightly infected trees and killing heavily infected trees. Effects of this treatment were monitored to 2003 with two, nearly adjacent, 4-ha plots. Typical forest-wide treatment was conducted on one of these plots; the other was left untreated for comparison.

The treated stand was inventoried 12 times since 1949; the untreated stand was inventoried 11 times since 1950 (see Fig. 8, bottom two rows of panels). The untreated stand had an initial stem density of 10 stems ha^{-1} in 1950 (13 m^2 ha^{-1} basal area; 47 cm QMD). Mistletoe intensity (DMR) and severity (DMI) were 3.0 and 3.8 respectively. Over the next 50 years, this stand experienced a mix of large-tree mortality and ingrowth of new and advanced regeneration, some of which followed a prescribed burn in 1985. By 2003 the stand had about the same basal area as 1950 but over three times the density: 31 stems ha^{-1}, and a smaller QMD of 25 cm. In 1949, the treated stand began with 6 stems ha^{-1} (9 m^2 ha^{-1} basal area; 46 cm QMD) and intensity and severity of 3.1 and 3.7, respectively. The first three treatment entries reduced the density to 3 stems ha^{-1} and intensity and severity to <0.1 and 1.0, respectively. Subsequent growth of natural regeneration over the following decades brought the stand to a density of 52 stems ha^{-1} in 2003 (20 m^2 ha^{-1} basal area, 24 cm QMD). Over five decades, tree density (as stems and as basal area) and stem clumping increased for both stands. For the untreated stand, mistletoe contagion remained mostly unchanged, reflecting essentially a single, well-distributed population of mistletoe. Although initial mistletoe contagion on the treated stand was similar to that of the untreated stand, it displayed more extreme changes over time. Treatment first eliminated any pattern of mistletoe distribution when all but a few infected trees were pruned or killed. Later, mistletoe spread from the few, isolated, infected trees to the emerging saplings over 2 m tall, generating sharply defined patches.

For both stands, multiple simulations were made; each beginning at an inventory year and terminating in 2008 (see Fig. 8, upper rows of panels). Stocking was adjusted each inventory year with a scheduled removal and planting to account for observed mortality and regeneration not simulated by the epidemiology model. The observed and simulated levels for stems and basal area are therefore coincident by design to highlight the effects of mistletoe dynamics on the

key dwarf mistletoe indicators (Fig. 8), rather than background mortality, regeneration, and ingrowth.

Generally, the trajectories of simulated dwarf mistletoe dynamics for a treated and an untreated stand track well with observed indicators (Fig. 8). While mistletoe severity (DMI) can vary more from cycle to cycle when there are few infected trees, most simulations also track spread and intensification well as interactions take place between overstory and understory trees. Repeated entries in the treated stand reduce mistletoe intensity (DMR) to a sparse incidence (% Infected) of trees with low infection severity, but these infested trees provide sufficient inoculum to infect the emerging regeneration. Especially after treatment, latent infections (or trees incorrectly classified as mistletoe-free in the inventory) also contribute to subsequent infection. A notable example can be seen in the treatment simulation beginning in 1949, in which some spread takes place before the first treatment, later causing greater spread (increased incidence) throughout the simulation. This behavior is the result of latent infections which are invisible when the first treatment is made in 1954, but which subsequently mature, reproduce and provide inoculum for new infections. In contrast, subsequent FVS simulations that begin in later years do not include any latent infections and consequently have lower measures of initial infestation. For the untreated stand, mistletoe intensity continues to be high for several decades and then declines as old-growth trees die and regeneration appears. Simulations track severity and incidence well; differences between observed and simulated levels of each are complementary so that simulated intensity best tracks intensity (recall Eq. (1)). Simulations begun early in this stand's history tend to under-estimate mistletoe severity (intensification) and over-estimate incidence (spread); projections for later cycles in longer simulations, and simulations begun later in history, tend to converge on observed levels. The magnitude of the early differences is not large enough to suggest a need to revise default parameters, but calibration based on additional research and observation would be justified.

5. Conclusions

Although dwarf mistletoes are important plant pathogens in many conifer forests of Western North America, they are often overlooked and their long-term, cumulative effects are unrecognized. Whether managed for commodities or ecological services, silviculture is a practical management tool for mistletoe-infested stands (Muir and Geils, 2002). Given the difficulty of predicting long-term response to treatment, simulation models are especially useful for these stands. We identify the key features of the mistletoe–conifer system as life history, ballistics, and contagion and model mistletoe dynamics as change in DMR, mistletoe intensity. Important elements of life history are a lag from infection to dispersal, light-mediated control over reproduction, and effects of fungal disease. Observations and physics set the range of ballistic seed dispersal at about 14 m. Because there are a large number of seeds disseminating in a complex, heterogeneous environment, a probabilistic, all-paths approach is used. The heterogeneous environment consists of crowns of trees that function as infection sources, targets, and screens, variously arranged both vertically and horizontally. We simplify this complexity by reduction to measures of canopy opacity (for light and for seed interception), stem clumping, and mistletoe contagion. The epidemiological model has modest data requirements that can be easily met in practice, and also has the flexibility to accommodate a range of stand compositions and management options. Through a series of exercises, the mistletoe model as attached to FVS demonstrates a variety of behaviors that have significant implications for model use. Stand inventories typically do not include DMR by crown-third; one relevant test shows little model sensitivity to initial mistletoe distribution by crown-third, implying that whole-tree, inventory DMR is adequate. In contrast, canopy opacity, stem clumping, and mistletoe contagion can be derived (or approximated) from most stand inventories. Changes in these can result in very different projections, implying these factors should be considered. Simulations using this model can track well the observed, long-term dynamics of mistletoe populations. There remain needs and opportunities for model development, calibration, and validation. First, the model could make fuller use of the spatial information available in the form of inventory sample points, rather than using stand-averages to compute opacity and drive the selection of neighborhood trees. A revised interface with the growth model could create a better link between crown and canopy characteristics and the longevity of mistletoe infection. This elaboration would facilitate development of a broom sub-model useful to assess fuel hazard and wildlife habitat. The lag from infection to first seed dispersal and occurrence of subsequent reproductive bouts vary by mistletoe species and environmental factors such as drought and fungal disease. Sensitivity analyses and field research could assist with calibration and refinement of default values. Over the past decade, numerous mistletoe-infested stands have been sufficiently monitored to serve for benchmark comparisons such as illustrated here with the GC stands. Nonetheless, the present dwarf mistletoe epidemiology model can now provide managers with a practical tool for simulating mistletoe spread and intensification in stands of complex composition and structure.

Acknowledgments

We express our appreciation to the more than thirty foresters, plant pathologists and modelers (Robinson et al., 1994) who originally contributed time and expertise to the conception of this model, developed under contract for the USDA Forest Service, Fort Collins, Colorado. In particular, Glenn Sutherland provided very helpful early discussions of spatial approaches. Studies of model behavior in hemlock silvicultural systems were supported through contracts to J.A. Muir of the B.C. Ministry of Forests. Subsequent elaboration of the life history and biological control portion of the model was supported through a contract to B.J. van der Kamp and S.F. Shamoun, University of B.C. Department of Forestry and Natural Resources Canada Pacific Forestry Centre, respectively. We thank D.C. Shaw for use of data obtained from the Wind River Canopy Crane Research Facility, a cooperative scientific program of the University of Washington, U.S. Forest Service Pacific North-

west Research Station and Gifford Pinchot National Forest, located on the Wind River Experimental Forest. The Earthwatch Institute and Durfee Foundation supported plot establishment and measurement through the Student Challenge Award Program. We also thank R. Obedzinski of the Gifford Pinchot National Forest for FVS calibration advice for the WRCC inventory. J.J. Smith, Northern Arizona University, conducted preliminary examination of contagion, stem clumping, and mistletoe patches under a cooperative venture funded by the Rocky Mountain Research Station. Data from the Grand Canyon sites were collected through long-term cooperation and support by the U.S. Department of Interior, National Park Service, Grand Canyon National Park and U.S. Department of Agriculture, Forest Service—including the Rocky Mountain Research Station, Forest Health Protection (Special Technology Development Project R6-2003-05), and Southwest Region. Manuscript preparation was supported by a contract with the Rocky Mountain Research Station and through internal research funding by ESSA Technologies Ltd. We thank our several reviewers for their helpful suggestions and Kelly Robson for help in preparing the figures.

REFERENCES

Allen, T.F.H., Starr, T.B., 1982. Hierarchy: Perspectives for Ecological Complexity. University of Chicago Press, Chicago, IL, 310 pp.

Baker, F.A., French, D.W., Rose, D.W., 1982. DMLOSS: a simulator of losses in dwarf mistletoe infested black spruce stands. Forest Sci. 28, 590–598.

Bickford, C.P., Kolb, T.E., Geils, B.W., 2005. Host physiological condition regulates parasitic plant performance: *Arceuthobium vaginatum* subsp. *cryptopodum* on *Pinus ponderosa*. Oecologia 146, 179–189, doi:10.1007/s00442-005-0215-0.

Bloomberg, W.J., Smith, R.B., Van der Wereld, A., 1980. A model of spread and intensification of dwarf mistletoe infection in young western hemlock stands. Can. J. Forest Res. 10, 42–52.

Brandt, J.P., Hiratsuka, Y., Pluth, D.J., 2005. Germination, penetration, and infection by *Arceuthobium americanum* on *Pinus banksiana*. Can. J. Forest Res. 35, 1914–1930, doi:10.1139/X05-113.

Chen, C., Marsden, M., Taylor, J.E., 1993. Sensitivity analysis of the interim dwarf mistletoe impact modeling system for the user. Rep. MAG-93-10. U.S. Department of Agriculture, Forest Service, Forest Pest Management, Methods Application Group, Fort Collins, CO, 13 pp.

Crookston, N.L., Stage, A.R., 1993. Predicting tree growth and development in patchy stands to simulate group selection silviculture. In: Interior Cedar-Hemlock-White Pine Forests: Ecology and Management, Spokane, WA, March 2–4, 1993. Department of Natural Resource Sciences, Washington State University, Pullman, WA, pp. 285–291.

David, L.R., 2005. Dwarf mistletoe impact modeling system, User guide and reference manual, nonspatial model, 2005 update. Unpublished report. U.S. Department of Agriculture, Forest Service, Forest Health Technology Enterprise Team, Fort Collins, CO, 73 pp., May 4, 2006. Available: http://www.fs.fed.us/foresthealth/technology/d_mod/DM_User_Guide_2005_nonspatial.pdf.

Dixon, G.E. (comp.), 2002. Essential FVS: a user's guide to the Forest Vegetation Simulator. Internal report. U.S. Department of Agriculture, Forest Service, Forest Management Service Center, Fort Collins, CO, 204 pp. [last revised: January 2006], May 4, 2006. Available: http://www.fs.fed.us/fmsc/fvs/documents/gtrs_essentialfvs.php.

Dixon, G.E., Hawksworth, F.G., 1979. A spread and intensification model for southwestern ponderosa pine. Forest Sci. 25, 43–52.

Edminster, C.B., Mower, H.T., Mathiasen, R.L., Schuler, T.M., Olsen, W.K., Hawksworth, F.G., 1990. GENGYM: a variable density stand table projection system calibrated for mixed conifer and ponderosa pine stands in the Southwest. Res. Pap. RM-297. U.S. Department of Agriculture, Forest Service, Rocky Mountain Forest and Range Experiment Station, Fort Collins, CO, 32 pp.

Feynman, R.P., 1985. QED: The Strange Theory of Light and Matter. Princeton University Press, Princeton, NJ, 158 pp.

Geils, B.W., Mathiasen, R.L., 1990. Intensification of dwarf mistletoe on southwestern Douglas-fir. Forest Sci. 36, 955–969.

Geils, B.W., Cibrián Tovar, J., Moody, B. (Tech. Coords.), 2002. Mistletoes of North American Conifers. Gen. Tech. Rep. RMRS-GTR-98. U.S. Department of Agriculture, Forest Service, Rocky Mountain Research Station, Ogden, UT, 123 pp., May 4, 2006. Available: http://www.fs.fed.us/rm/pubs/rmrs_gtr098.pdf.

Hawksworth, F.G., 1959. Ballistics of dwarf mistletoe seeds. Science 130, 504.

Hawksworth, F.G., 1961. Dwarfmistletoe of ponderosa pine in the Southwest. Tech. Bull. 1246. U.S. Department of Agriculture, Washington, DC, 112 pp.

Hawksworth, F.G., 1965. Life tables for two species of dwarfmistletoes. I. Seed dispersal, interception, and movement. Forest Sci. 11, 142–151.

Hawksworth, F.G., 1973. On a new power source. J. Irreproducible Results 20, 20.

Hawksworth, F.G., 1977. The 6-class dwarf mistletoe rating system. Gen. Tech. Rep. GTR-RM-48. U.S. Department of Agriculture, Forest Service, Rocky Mountain Forest and Range Experiment Station, Fort Collins, CO, 7 pp.

Hawksworth, F.G., Shaw III, C.G., 1984. Damage and loss caused by dwarf mistletoes in coniferous forests of western North America. In: Wood, R.K.S., Jellis, G.J. (Eds.), Plant Diseases: Infection, Damage and Loss. Blackwell Scientific Publications, Oxford, pp. 285–297.

Hawksworth, F.G., Wiens, D., 1996. Dwarf mistletoes: Biology, pathology, and systematics. Agric. Handb. 709. U.S. Department of Agriculture, Forest Service, Washington DC, 410 pp., May 4, 2006. Available: http://www.rmrs.nau.edu/publications/ah_709/.

Hawksworth, F.G., Williams-Cipriani, J.C., Eav, B.B., Geils, B.G. [sic], Johnson, R.R., Marsden, M.A., Beatty, J.S., Schubert, G.D., Robinson, D.C.E., 1995. Dwarf mistletoe impact modeling system, user's guide and reference manual. Rep. MAG-95-2. U.S. Department of Agriculture, Forest Service, Forest Pest Management, Methods Application Group, Fort Collins, CO, 120 pp.

Higgins, S.I., Richardson, D.M., Cowling, R.M., 2001. Validation of a spatial simulation of a spreading alien plant population. J. Appl. Ecol. 38, 571–584, doi:10.1046/j.1365-2664.2001.00616.x.

Hinds, T.E., Hawksworth, F.G., 1965. Seed dispersal velocity in four dwarfmistletoes. Science 148, 517–519.

Korstian, C.F., Long, W.H., 1922. The western yellow pine mistletoe. Agric. Bull. 1112. U.S. Department of Agriculture, Washington, DC, 35 pp.

Lightle, P.C., Hawksworth, F.G., 1973. Control of dwarf mistletoe in a heavily used ponderosa pine recreation forest, Grand Canyon, Arizona. Res. Pap. RM-106. U.S. Department of Agriculture, Forest Service, Rocky Mountain Forest and Range Experiment Station, Fort Collins, CO, 22 pp.

Maffei, H., Stone, J., David, L., Gregg, T., Adams, J., Geils, B., 1999. Development of the understory enhancement for the dwarf mistletoe spread and intensification model. In: Trummer, L. (Comp.), Proceedings of the 46th Western International Forest

Disease Work Conference, Reno, NV, September 28–October 2, U.S. Department of Agriculture, Forest Service, State and Private Forestry, Anchorage, AK, pp. 37–46.
Maloney, P.E., Rizzo, D.M., 2002. Dwarf mistletoe–host interactions in mixed-conifer forests in the Sierra Nevada. Phytopathology 92, 597–602.
Marsden, M.A., Shaw, C.G., III, Morrison, M., 1993. Simulation of management options for stands of Southwestern ponderosa pine attacked by Armillaria root disease and dwarf mistletoe. Res. Pap. RP-RM-308. U.S. Department of Agriculture, Forest Service, Rocky Mountain Forest and Range Experiment Station, Fort Collins, CO, 5 pp.
McNamee, P.J., Lekstrum, T., Bunnell, P., 1990. A modeling plan for dwarf mistletoe: Results of a workshop. Unpublished report prepared by ESSA Ltd., Vancouver, BC for Methods and Application Group, U.S. Forest Service, Fort Collins, CO, 33 p. Report on file at ESSA Technologies.
Mitchell, K.J., 1975. Dynamics and simulated yield of Douglas-fir. Forest Sci. Monogr. 17, 39.
Moeur, M., 1985. COVER: a user's guide to the CANOPY and SHRUBS extension of the Stand Prognosis Model. Gen. Tech. Rep. INT-190. U.S. Department of Agriculture, Forest Service, Intermountain Research Station, Ogden, UT, 49 pp., May 4, 2006. Available: http://www.fs.fed.us/fmsc/ftp/fvs/docs/gtr/cover.pdf.
Muir, J.A. and Geils, B.W., 2002. Management strategies for dwarf mistletoe: Silviculture. In: Geils, B.W., Cibrián Tovar, J., Moody, B. (Tech. Coords.). Mistletoes of North American Conifers. Gen. Tech. Rep. RMRS-GTR-98. U.S. Department of Agriculture, Forest Service, Rocky Mountain Research Station, Ogden, UT, pp. 83–94. May 4, 2006. Available: http://www.fs.fed.us/rm/pubs/rmrs_gtr098.pdf.
Myers, C.A., Hawksworth, F.G., Stewart, J.L., 1971. Simulation yields of managed, dwarf mistletoe-infested lodgepole pine stands. Res. Pap. RP-RM-72. U.S. Department of Agriculture, Forest Service, Rocky Mountain Forest and Range Experiment Station, Fort Collins, CO, 15 pp.
Nicholls, T.H., Egeland, L., Hawksworth, F.G., 1991. Birds of the Fraser Experimental Forest, Colorado and their role in dispersing lodgepole pine dwarf mistletoe. Colorado Field Ornithologists 23, 3–12.
Okubo, A., Levin, S.A., 1989. A theoretical framework for data analysis of wind dispersal of seeds and pollen. Ecology 70, 329–338.
Parker, G.G., 1997. Canopy structure and light environment in an old-growth Douglas-fir/western hemlock forest. Northwest Sci. 71, 261–270.
Parker, T.J., Mathiasen, R.L., 2004. A comparison of rating systems for dwarf mistletoe-induced witches' brooms in ponderosa pine. Western J. Appl. Forest. 19, 54–59.
Parmeter, J.R., Jr. 1978. Forest stand dynamics and ecological factors in relationship to dwarf mistletoe spread, impact, and control. In: Scharpf, R.F., Parmeter, Jr., J.R. (Tech. Coords.). Proceedings of the Symposium on dwarf mistletoe control through forest management, 11–13 April 1978. Berkeley, CA. Gen. Tech. Rep. GTR-PSW-31. U.S. Department of Agriculture, Forest Service, Pacific Southwest Forest and Range Experiment Station, Berkeley, CA, pp. 16–30.
Reich, R.M., Mielke Jr., P.W., Hawksworth, F.G., 1991. Spatial analysis of ponderosa pine trees infected with dwarf mistletoe. Can. J. Forest Res. 21, 1808–1815.
Robinson, D.C.E., Sutherland, G.D., 1993. The new dwarf mistletoe spread and intensification model: model review workshop report. Unpublished draft report prepared by ESSA Ltd., Vancouver, BC for USDA Forest Service, Methods and Application Group, Fort Collins, CO, 92 pp. Report on file at ESSA Technologies.
Robinson, D.C.E., Sutherland, G.D., 1995. The new dwarf mistletoe spread and intensification model: model description. Unpublished report prepared by ESSA Technologies Ltd., Vancouver, BC for U.S. Department of Agriculture, Forest Service, Methods Application Group, Fort Collins CO, 38 pp., Report on file at ESSA Technologies.
Robinson, D.C.E., Sutherland, G.D., Bunnell, P., Fairweather, M.L., Shubert, G., Taylor, J.E., Geils, B.W., 1994. The new dwarf mistletoe spread and intensification model: Final model review workshop report. Unpublished report prepared by ESSA Ltd., Vancouver, BC for USDA Forest Service, Methods Application Group, Fort Collins, CO, 26 pp., Report on file at ESSA Technologies.
Robinson, D.C.E., Geils, B.W., Muir, J.A., 2002. Spatial statistical model for the spread and intensification of dwarf mistletoe within and between stands. In: Crookston, N.L., Havis, R.N. (Comps.). Second Forest Vegetation Simulator Conference, 12–14 February 2002. Fort Collins, CO. Proc. RMRS-P-25. U.S. Department of Agriculture, Forest Service, Rocky Mountain Research Station, Ogden, UT, pp. 178–185, May 4, 2006. Available: http://www.fs.fed.us/rm/pubs/rmrs_p025/rmrs_p025_178_188.pdf.
Robinson, D.C.E., Geils, B.W., Muir, J.A., 2003. A spatial statistical model for the spread of dwarf mistletoe within managed stands. In: Stone, J., Maffei, H. (Comps.). Proceedings of the 50th Western International Forest Disease Work Conference, October 7–11, 2002. Powell River, BC. U.S. Department of Agriculture, Forest Service, Central Oregon Service Center, Bend, OR, pp. 131–140.
Seem, R.C., 1984. Disease incidence and severity relationships. Annu. Rev. Phytopathol. 22, 133–150.
Shamoun, S.F., Ramsfield, T.D., van der Kamp, B.J., 2003. Biological control approach for management of dwarf mistletoes. NZ J. Forestry Sci. 33, 373–384.
Shaw, D.C., Weiss, S.B., 2000. Canopy light and the distribution of hemlock dwarf mistletoe (*Arceuthobium tsugense* [Rosendahl] G.N. Jones subsp. tsugense) aerial shoots in an old-growth Douglas-fir/western hemlock forest. Northwest Sci. 74, 306–314.
Shaw, D.C., Chen, J., Freeman, E.A., Braun, D.M., 2005. Spatial and population characteristics of dwarf mistletoe infected trees in an old-growth Douglas-fir/western hemlock forest. Can. J. Forest Res. 35, 990–1001, doi:10.1139/X05-022.
Smith, R.B., 1973. Factors affecting dispersal of dwarf mistletoe seeds from an overstorey western hemlock tree. Northwest Sci. 47, 9–19.
Smith, R.B., 1985. Hemlock dwarf mistletoe biology and spread. In: Muir, J.A. (Ed.), Workshop on Management of Hemlock Dwarf Mistletoe, August 15–16, 1983. Burnaby, BC. Rep. 4. British Columbia Ministry of Forests, Forest Pest Management, Victoria, BC, pp. 4–10.
Stage, A.R., 1973. Prognosis model for stand development. Res. Pap. INT-137. U.S. Department of Agriculture, Forest Service, Intermountain Forest and Range Experiment Station, Ogden, UT, 32 pp.
Strand, M.A., Roth, L.F., 1976. Simulation model for spread and intensification of western dwarf mistletoe in thinned stands of ponderosa pine saplings. Phytopathology 66, 888–895.
Watson, D.M., 2001. Mistletoe—a keystone resource in forests and woodlands worldwide. Annu. Rev. Ecol. Systemat. 32, 219–250, doi:10.1146/annurev.ecolsys.32.081501.114024.
Wicker, E.F., Shaw, C.G., 1967. Target area as a klendusic factor in dwarf mistletoe infections. Phytopathology 57, 1161–1163.
Willocquet, L., Savary, S., 2004. An epidemiological simulation model with three scales of spatial hierarchy. Phytopathology 94, 883–891.